To appear in *Philosophical Magazine*
Vol. 00, No. 00, Month 20XX, 1–11

Structural modifications and electron beam damage in aluminium alloy precipitate θ'–Al_2Cu

Sigurd Wenner[a*], Jesper Friis[b], Calin D. Marioara[b], Sigmund J. Andersen[b] and Randi Holmestad[a]

[a]*Department of Physics, NTNU - Norwegian University of Science and Technology, Trondheim NO-7491, Norway;* [b]*Materials and Chemistry, SINTEF, Trondheim NO-7491, Norway*

(*Received 00 Month 20XX; accepted 00 Month 20XX*)

The θ'–Al_2Cu phase in an Al–4Zn–2Cu–1Mg–0.7Si (wt.%) alloy was investigated by means of scanning transmission electron microscopy. With our specific alloy composition, the phase is often formed with stacking faults on $\{101\}_{\theta'}$ and $\{001\}_{\theta'}$ planes. The stacking faults on $\{101\}_{\theta'}$ planes are often regularly spaced and create a previously unreported superstructure. Structural damage by electron irradiation is observed, even at a low acceleration voltage of 80 kV. The damage is more pronounced in the θ' precipitates with stacking faults, which agrees with theoretical calculations of knock-on scattering cross-sections. These two very different forms of disruptions of the θ' structure are linked to its spacious interstitial sites and the ease at which Cu atoms diffuse into and between them.

Keywords: alloys, precipitation, structural transitions, irradiation effects, transmission electron microscopy

1. Introduction

Aluminium alloys with copper as the main alloying element brought the first discovery of age-hardening [1], which was later explained by precipitation of Cu-rich nano-precipitates [2]. The main hardening phases of this system are θ'' and θ', with structures more similar to the fcc–Al lattice than to the equilibrium precipitate phase θ [3]. The aluminium crank case used in the first flight by the Wright brothers was investigated with modern methods two decades ago and was found to contain a high density of Guinier–Preston-zones [4] and a few θ' precipitates [5]. The θ'' phase, sometimes called GPII, is a curious constellation of $\{001\}_{\mathrm{Al}}$ planes with Al substituted by Cu, spaced 808 pm (four Al planes) apart, making its composition Al_3Cu [6]. The phase has a plate-shaped morphology. The θ' phase may emerge from existing θ'' precipitates or nucleate independently. The interface planes between θ' and fcc–Al are identical to the θ'' Cu planes [7], but the interior $\{001\}_{\theta'}$ Cu planes are only 290 pm apart, with half of the Cu atoms missing. One $\{001\}$ plane of fcc–Al are kept in-between the Cu planes, such that the bulk composition is Al_2Cu. The firmly established Silcock model for θ' gives the phase a tetragonal space group $I\bar{4}m2$ and lattice parameters $a = 404$ pm and $c = 580$ pm [3, 8]. The majority

*Corresponding author. Email: sigurd.wenner@ntnu.no

of θ' plates have the orientation relationship $\{001\}_{\theta'}||\{001\}_{\mathrm{Al}}$, $\langle 100\rangle_{\theta'} \,||\, \langle 100\rangle_{\mathrm{Al}}$, but plates with $\{001\}_{\theta'}||\{011\}_{\mathrm{Al}}$, $\langle 100\rangle_{\theta'} \,||\, \langle 100\rangle_{\mathrm{Al}}$ have also been observed [9].

Many old and new studies are concerned with the atomic structure of θ'. Although its bulk structure was solved by X-ray diffraction [8], transmission electron microscopy (TEM) and electron diffraction have a superior spatial resolution, and are the best suited methods for studying individual θ' precipitates embedded in Al. We present here TEM observations of two types of stacking faults in θ' precipitates in an Al–4Zn–2Cu–1Mg–0.7Si (wt.%) alloy, and show how the faults can build a regular superstructure. We also discuss how the high mobility of Cu atoms have the effect of θ' being susceptible to damage from electron irradiation in a TEM instrument.

2. Experimental methodology

High-angle annular dark-field scanning TEM (HAADF–STEM) was chosen as an electron imaging technique since it produces readily interpretable micrographs independent of specimen thickness. Moreover, it gives a high contrast between elements of different atomic number (e.g. between Al and Cu). The experiments were performed with a JEOL ARM-200F cold field emission gun microscope with probe and image spherical aberration correctors, and a Centurio EDS detector. The beam convergence angle was 27 mrad and the collection angles of the HAADF detector were 42–178 mrad. To address beam damage issues, two acceleration voltages were used, 200 kV and 80 kV, with respective probe currents $\approx$ 21.0 pA and $\approx$ 6.5 pA. The composition of the studied alloy was 4.0 % Zn, 2.0 % Cu, 1.0 % Mg, 0.7 % Si, 0.55 % Mn and 0.20 % Fe by weight. Alloys with a reduced Zn content (1.0 and 0.0 wt.%) were also briefly investigated. After extrusion into cylindrical rods of 20 mm diameter, samples were heated at 400 °C for 1 hour, quenched in water and directly aged at 150 °C for 32 days. In addition to θ', several other phases were present: see [10] for details on the microstructure evolution. TEM specimens were thinned by electrolyte polishing at 20 V, using a mixture of 1/3 HNO_3 and 2/3 CH_3OH cooled to −25 °C.

3. Computational methodology

The energetics of interstitial self-diffusion of Cu in θ' was evaluated by means of density functional theory (DFT) calculations. For this purpose, we utilized the popular Vienna ab initio simulation package (VASP) software [11, 12], with the projector-augmented wave (PAW) method [13] and Perdew–Burke–Ernzerhof exchange correlation potentials [14]. A Γ-centered k-point mesh was used in all calculations, with a maximal k-point distance of 0.25 $\mathrm{Å}^{-1}$ and energy cut-off above 340 eV. For structural relaxations we applied the Methfessel–Paxton method [15] of order one and a smearing factor of 0.2, while the tetrahedron method with Blöchl corrections was used for energy calculations. The nudged elastic band (NEB) approach was used to find the saddle point in energy along the path of a Cu atom from initial to final position, while relaxing the surrounding atoms. The enthalpies were evaluated from configurations found by climbing image NEB [16, 17], to find the atomic diffusion barrier, or critical displacement energy, T_{d}.

Electron irradiation is known to initiate diffusion jumps and create Frenkel defects

(vacancy–interstitial pairs) through the knock-on damage process [18]. The rate of damaging depends on the diffusion barrier and the incoming electron energy, and can be estimated from relativistic electron–atom scattering cross-sections. The electron energy has to be above a certain threshold for knock-on damage to occur. We follow an approach similar to what has been used to predict beam damage of Al_3(Li, Sc, Zr) particles in Al [19]. The solid angle-integrated elastic scattering cross-section σ_d can be obtained from the Mott model [19, 20]:

$$\begin{aligned}\sigma_\mathrm{d} &= 4\pi\frac{Z^2a_0^2E_\mathrm{R}^2}{m_e^2}\cdot\frac{1-\beta^2}{\beta^4} \\ &\times \left[\kappa-1-\beta^2\ln\kappa+\pi\frac{Z}{137}\beta(2\sqrt{\kappa}-2-\ln\kappa)\right],\end{aligned} \tag{1}$$

where Z is the atomic number of the scattering atom, a_0 is the Bohr radius, E_R and m_e are the Rydberg energy and the electron mass in eV, while β is the relativistic electron speed in units of the speed of light c. Further, $\kappa = T_\mathrm{max}/T_\mathrm{d}$, where T_max is the maximum transferable energy (through perfect backscattering) between the incident electron and an atom in the specimen:

$$T_\mathrm{max} = 4\frac{m_e}{m_\mathrm{atom}}\left(1+\frac{U}{2m_e}\right)U, \tag{2}$$

where units of eV are used for T_max, the electron and atom masses m_e and m_atom, and the acceleration potential of the electron microscope U. Using the same convention,

$$\beta = \sqrt{1-\frac{m_e^2}{(U+m_e)^2}}. \tag{3}$$

For our case of knock-on damage, the critical displacement energy T_d is equal to the diffusion energy of an atom into a neighboring interstitial site. It is the most decisive parameter for the onset of electron beam damage in a TEM. For fcc-Al, $T_\mathrm{d} \approx 16$ eV [21], which gives a positive σ_d above ≈ 180 keV. For Cu in θ', we have calculated the critical displacement energy by NEB–DFT calculations. The relevant jumps to interstitial sites go half a unit cell along $\langle 110\rangle_{\theta'}$ and $\langle 001\rangle_{\theta'}$ directions (see Fig. 2).

4. Results

4.1. *Stacking faults*

Large (30–100 nm in projected length) θ' plates were imaged edge-on by HAADF–STEM. Most of these assumed the $\{001\}_{\theta'}||\{001\}_\mathrm{Al}$ orientation relationship [Fig. 1(a–d)], while a small portion had the $\{001\}_{\theta'}||\{011\}_\mathrm{Al}$ relationship [Fig. 1(e)]. Two types of stacking faults were observed, on $\{101\}_{\theta'}$ and $\{001\}_{\theta'}$ planes. Fig. 1(ab) shows each of the two types, and Fig. 1(c) shows a precipitate with both faults. Fig. 1(d) shows how a θ' with $\{101\}_{\theta'}$ faults appear when not viewed parallel to the fault planes. In all images the electron beam is parallel to the $\langle 001\rangle_\mathrm{Al}$ zone axis. The projected spacings of the atomic columns in θ' are longer in the $\langle 011\rangle_\mathrm{Al}$ orientation,

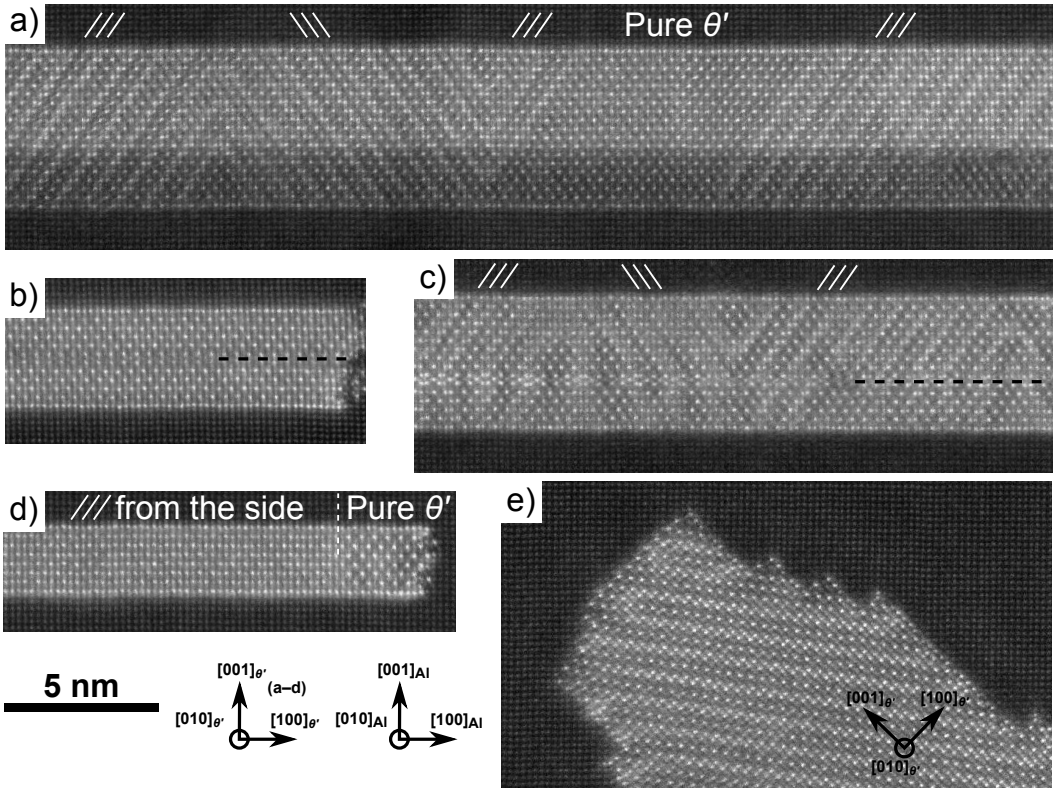

Figure 1. (a–d) HAADF–STEM images acquired at 200 kV of θ' plates (seen edge-on) with a $\{001\}_{\theta'}||\{001\}_{\mathrm{Al}}$ orientation, containing stacking faults along (a) $\{101\}_{\theta'}$ planes, (b) $\{001\}_{\theta'}$ planes, and (c) both. Bright atomic columns means a high Cu content. The bottom side of (a) is dark because the precipitate has a horizontal ledge, leaving part of the precipitate thinner and overlapped with the Al lattice. The precipitate in (d) probably has stacking faults on $\{101\}_{\theta'}$ planes which are not parallel to the viewing direction. (e) A precipitate in a $\{001\}_{\theta'}||\{011\}_{\mathrm{Al}}$ orientation, which also has $\{101\}_{\theta'}$ stacking faults.

which would make lattice imaging easier, but the $\{101\}_{\theta'}$ stacking faults would not be observable in this orientation.

The faults on $\{001\}_{\theta'}$ planes can in their most basic form be described by a slip motion half a unit cell in a $\langle 110\rangle_{\theta'}$ direction. Such a translation always conserves the Al positions in both θ' and fcc–Al. In Fig. 1(c), some bright Al columns along the fault indicate the presence of partial Cu occupancy. This is shown schematically in Fig. 2. The diagonal faults on $\{101\}_{\theta'}$ can not be generated by a simple symmetry operation as they require extra columns of Cu. However, a single fault can be described as Cu atoms making jumps half a unit cell in either the $\langle 110\rangle_{\theta'}$ or the $\langle 001\rangle_{\theta'}$ direction in part of the structure, see Fig. 2. The $\{101\}_{\theta'}$ faults often appear with regular spacings of 828 pm, effectively creating a superstructure with a larger unit cell (see Fig. 3). As this modified structure appears commonly in our alloy, we refer to it in the further as θ'_{D} (D for diagonal). Full occupation according to the scheme of Fig. 3(b) would give an Al_5Cu_3 composition and the space group C2/m (or A2/m if one takes into account the *bc*-plane centering of the unit cell).

DFT calculations of the original and modified θ' unit cells were performed to estimate the bulk formation enthalpy. The enthalpy is -0.16 eV/atom for θ'_{D} and -0.15 eV/atom for θ', with Cu in solid solution used as the reference. The relaxed (minimum enthalpy) structures found here were used for the NEB calculations in the next section.

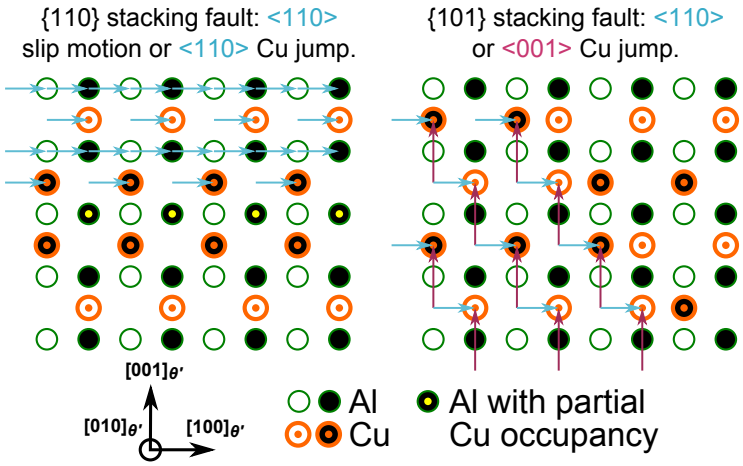

Figure 2. Schematic of how the two stacking faults observed in Fig. 1 can be generated by either slip motions of the whole structure or individual jumps of Cu atoms. White/black fill distinguishes atoms that are spaced 202 pm in the $[010]_{\theta'}$ direction.

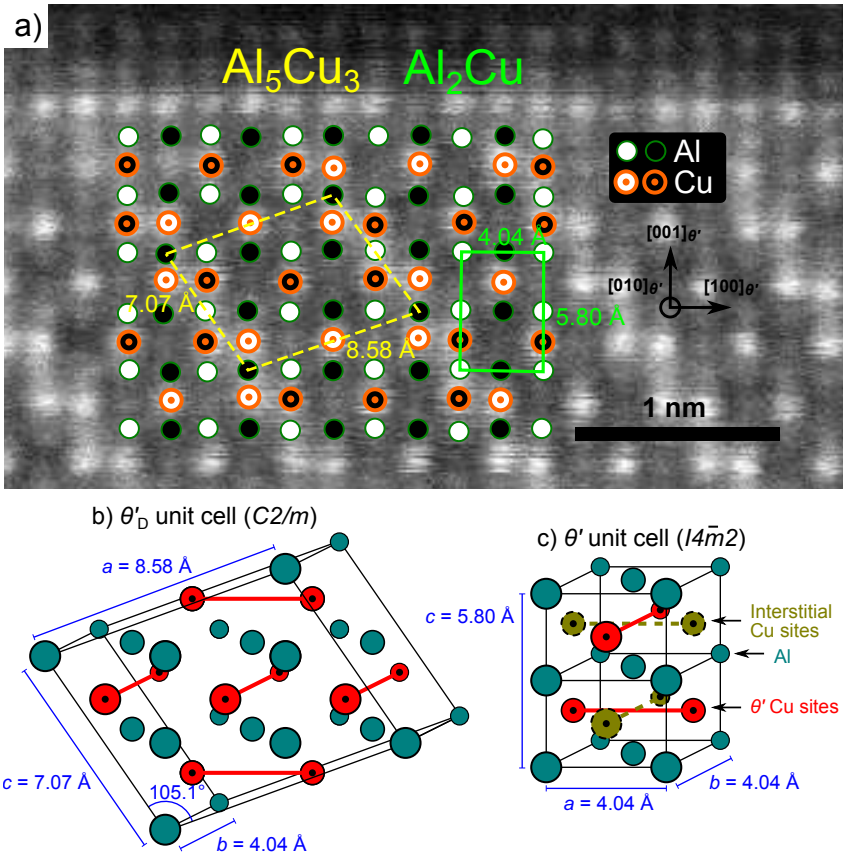

Figure 3. (Color online) (a) Drift-corrected HAADF–STEM image of a θ'_{D} precipitate, acquired at 80 kV. The overlay shows the atomic structure and unit cell of the pure and modified θ' structures. White/black fill distinguishes atoms that are spaced 202 pm in the viewing direction. (b) Three-dimensional model of the θ'_{D} unit cell. The structure is identical to θ' except that some Cu atoms are removed and others are added to the interstitial sites shown in (c).

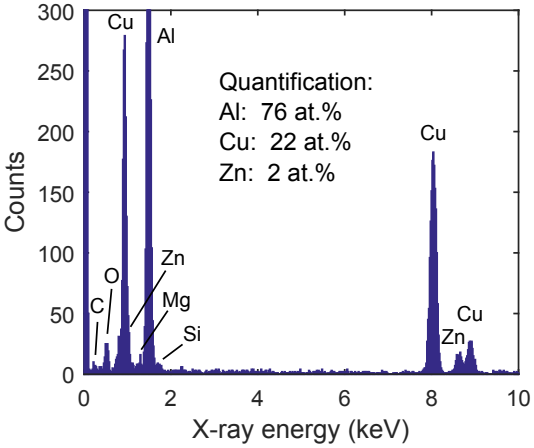

Figure 4. (Color online) Typical EDS spectrum from the bulk structure of a θ' precipitate, to show the presence of Zn in the bulk composition.

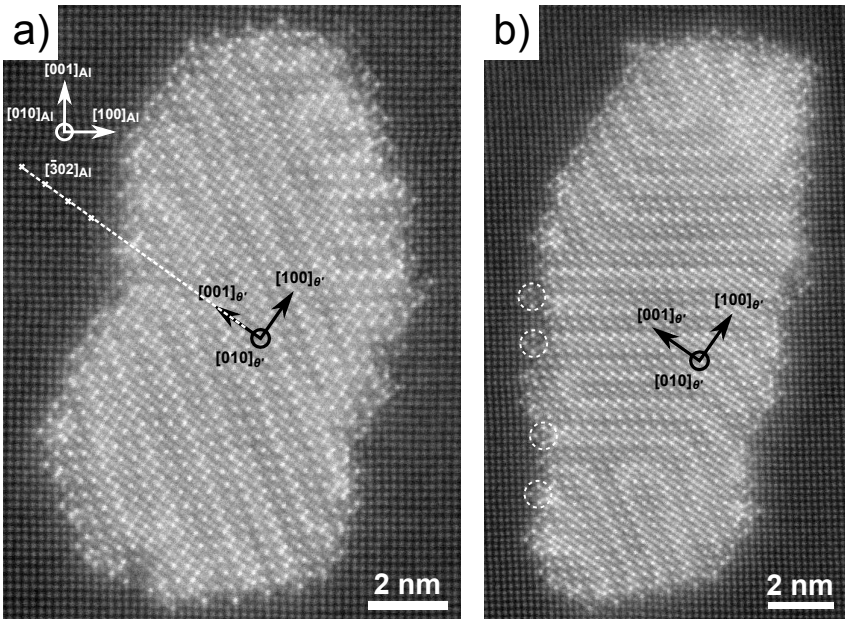

Figure 5. Two particles with the θ'_{D} structure, observed in an Al–2Cu–1Mg–0.7Si (wt.%) alloy. Their shape may be either arbitrary or rod-like with the main growth direction normal to the image plane. The dashed circles in (b) indicate the presence of what appears to be GPB-zone units from the Al–Cu–Mg system [22].

Compositionally, about 7% of the Cu atoms in the precipitates was replaced by Zn atoms, as measured by energy-dispersive X-ray spectroscopy (EDS). A typical EDS spectrum is seen in Fig. 4. STEM–EDS mapping was not attempted as this requires a high electron dose, which would alter the precipitate structure, as noted in the next section. All cases of faults in Fig. 1 were also found in alloys with 1.0 and 0.0 wt.% Zn (keeping 1.0% Mg and 0.7% Si), although the reduction in Zn content makes them significantly less common. A very special case of θ'_{D} particles was observed in the alloy with 0.0% Zn: These are either rod-like or arbitrarily shaped, and have the special orientation relationship $\{001\}_{\theta'} || \{023\}_{\mathrm{Al}}$, $\langle 100\rangle_{\theta'} \,||\, \langle 100\rangle_{\mathrm{Al}}$ (see Fig. 5).

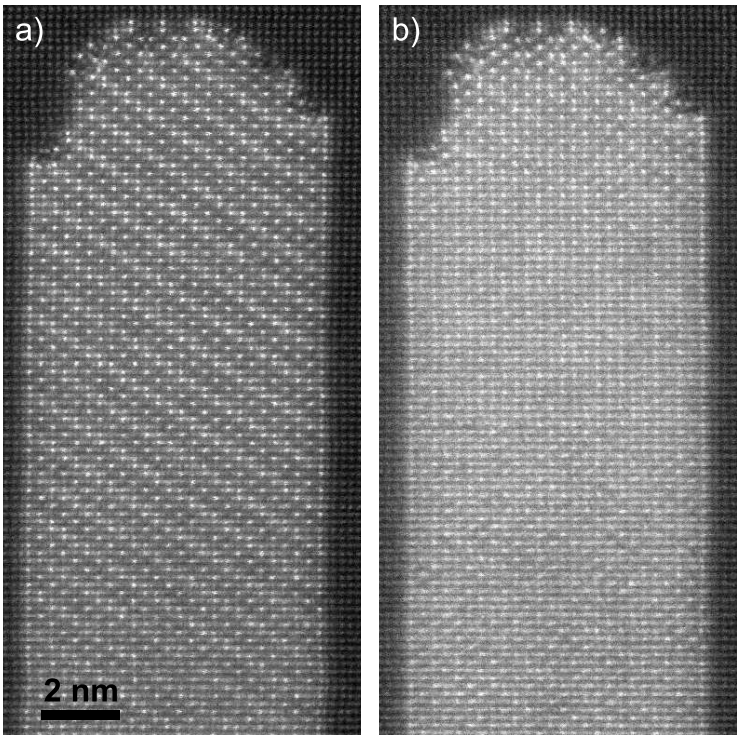

Figure 6. Two consecutive 15 second HAADF–STEM exposures of a θ'_{D} precipitate using 200 kV electrons. An electron dose of 1.5 pC/nm^2 has altered the atomic structure beyond recognition.

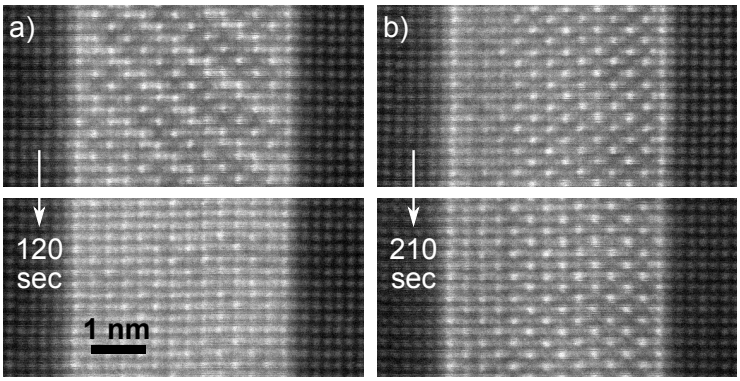

Figure 7. HAADF–STEM images at the start and end of some minutes of electron irradiation at 80 kV. Two locations on the same precipitate, with (a) θ'_{D} and (b) θ' structures. The total doses suffered by the precipitate are (a) 22 pC/nm^2 and (b) 37 pC/nm^2 in the lower images.

4.2. *Electron beam damage of θ'*

Although a 200 kV electron beam is above the threshold for knock-on damage in fcc–Al, the damage happens very slowly in a TEM. The same can not be said for the θ' phase, as seen from two consecutive STEM exposures at 200 kV of the same particle, which turn out completely different (Fig. 6). Electron beam induced Cu diffusion has transformed an ordered θ'_{D} phase to a structure where the original Cu sites and the interstitial sites probably have a uniform, random occupancy. The electron dose of each exposure, calculated here as probe current multiplied by time divided by scan area, was 1.5 pC/nm^2. Damage occurs both for the θ' and θ'_{D} phases,

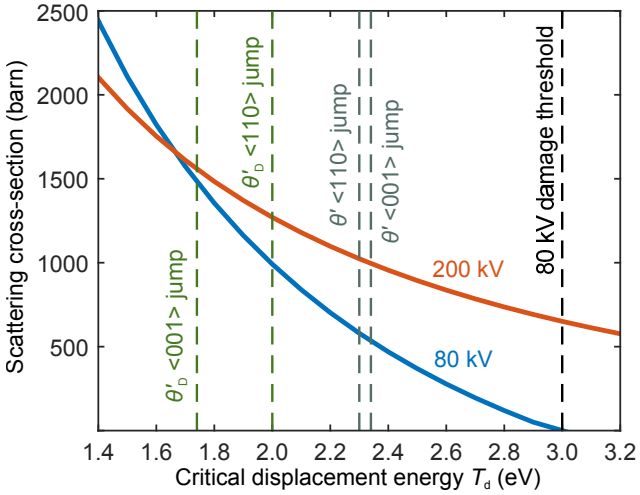

Figure 8. Scattering cross-sections for displacement of Cu atoms by electrons σ_d, calculated from Eq. (1) for the two relevant acceleration voltages. Atomic jumps in θ' and θ'_D can be activated by both 80 and 200 kV electrons.

and gives a projected appearance identical to that of $\{101\}_{\theta'}$ stacking faults along planes not parallel to the viewing direction, as in Fig. 1(d). When imaging with 80 kV electrons, the damaging rate decreases drastically. As shown in Fig. 7, after some minutes of beam exposure, the damage is apparent in θ'_D, but hardly seen at all in pure θ'.

The calculated energies required to initiate atomic diffusion in θ'/θ'_D lie in the range 1.74–2.34 eV, which is substantially lower than the 16 eV required in fcc–Al [21]. All values are shown in Fig. 8, together with scattering cross-sections for atomic displacement at 80 and 200 kV. The cross-section is greater for θ'_D and for 200 kV, which agrees qualitatively with the observed damage.

5. Discussion

Both types of stacking faults presented in Fig. 1 can be described as a redistribution of Cu atoms among the original and the interstitial sites, keeping the Al layers unchanged. The same type of faults were found in significantly larger θ' particles in pure Al–Cu alloys, probably with $\{100\}_{\theta'}$ fault planes [23, 24]. The θ'_D structure can be created by selectively removing 40% of the Cu from the θ' Cu positions while occupying 60% of the neighboring interstitial positions [the two types of sites are shown in Fig. 3(c)]. Occupying both sites fully in one layer yields the structure of the interface with fcc–Al. The unit cell of θ'_D [see Fig. 3(b)] has one more Cu atom than a corresponding volume of θ', which means it would be subjected to some compressive stress when embedded in Al. Similar changes of occupation between the original Cu sites and interstitial positions have been observed at the semi-coherent edges of θ' plates. This phenomenon was connected to the ease of Cu diffusion from the Al matrix into θ' [25]. According to our DFT results, the θ'_D superstructure has a slightly lower bulk enthalpy than θ'. Nevertheless, it is rarely found in its common plate-shaped form in alloys without Zn. The Zn content in the imaged particles seems to contribute to the energetic favorability of stacking faults and θ'_D, probably by reducing the interfacial enthalpy or the misfit with Al. The less coherent particles

in Fig. 5 seem to have their interface with Al partially composed of GPB-zone units, which contain Cu and Mg [22]. The interface structure is undoubtedly important for the ability of θ'_{D} to precipitate with an $\{001\}_{\theta'}||\{023\}_{\mathrm{Al}}$ orientation relationship. Finding the exact roles Zn, Mg and Si have in the formation of θ'_{D} is a subject for further computational studies.

What separates the θ' structure from e.g. fcc–Al in the context of Frenkel defects is that the Cu sites and the interstitial sites in θ' are equivalent, i.e. the crystal structure is invariant under an exchange of site type [see Fig. 3(c)]. This means that the stacking faults observed in θ' can be viewed as antiphase boundaries, with Cu atoms and vacancies exchanging places [24]. When a Cu atom occupies an interstitial site, its nearest-neighbor distances become 248 pm from Al atoms and 286 pm from other Cu atoms. The interstitial volume is 47.3 $\mathrm{Å}^3$, when defined by the geometrical shape with nearest-neighbor atoms as corners (a cuboid with Al corners in this case). This is large compared to the volume of the octahedral interstitial sites in fcc–Al (11.1 $\mathrm{Å}^3$) and the stable θ phase [3] (8.5 $\mathrm{Å}^3$). Consequently, by our DFT calculations, one Frenkel defect has the approximate energies 1.0 eV in θ' and 0.4 eV in θ'_{D}, compared to 4 eV [26] in fcc–Al. Cu diffusion in θ' is therefore an energetically cheap process, and defects such as the stacking faults discovered here may form, move and annihilate continuously during heat treatment (observed directly in [27]). Al atoms can of course also occupy the interstitial sites, but in order for them to stay there, a diffusion barrier must exist, and this requires longer and more tricky jumps.

The damage from electron irradiation observed in θ'-like particles are another consequence of high Cu mobility. Electron beam induced Cu diffusion can transform ordered $\theta'/\theta'_{\mathrm{D}}$ phases to a structure where the Cu appears uniformly distributed over inherent and interstitial Cu sites. The related calculations, presented in Fig. 8, say that 200 kV electrons are roughly twice as damaging to θ' as 80 kV electrons, and that 80 kV electrons damage θ'_{D} twice as fast as they damage θ'. This is not exactly as observed in Figs. 6 and 7, which hint at a much greater factor (note the differences in electron dose, written in the captions). Neither is the average number of interstitial jumps per atom f_{d} as expected for 80 kV. This number is obtained by multiplying the dose (in electrons/barn) with σ_{d} (the sum of both jump directions was used here), and yields $f_{\mathrm{d}} = 2.6$ for Fig. 6, indicating that all Cu atoms made 2.6 jumps on average, destroying the structure completely. However, for Fig. 7(b), $f_{\mathrm{d}} = 26$, although the precipitate has seemingly sustained little damage.

Beam damage from 80 kV electrons is seen from Fig. 8 to decline quickly with an increase of critical displacement energy T_{d}, up to the threshold energy at 3.0 eV. The above discrepancies could therefore be resolved with an upward adjustment of T_{d}. Moving all four jumps 0.6 eV to the right would for example put θ' close to the damage threshold while leaving θ'_{D} with a significant damaging rate, describing the very apparent sensitivity difference of the two structures seen in Fig. 7. One point worth raising is that our NEB calculation involved relaxing the atoms surrounding the jumping Cu atom for a smooth transition, while others have with reasonable results used a "sudden approximation", in which relaxation is omitted at the saddle point [19, 28]. Test calculations reveal that this raises our jump energies by about 1.6 eV, which brings all jumps safely past the damage threshold. A real beam-induced displacement can thus be best described as something in between the two extremes of full/no neighborhood relaxation. The Zn content in the precipitates in our alloys and the free sample surfaces of a TEM specimen may also influence T_{d} slightly.

6. Conclusion

We have investigated strengthening θ'–Al_2Cu precipitates in Al(–4Zn)–2Cu–1Mg–0.7Si (wt.%) alloys. Through high-resolution STEM imaging, we observe a structure consistent with the Silcock structural model found by X-ray diffraction. However, the spacious and easily accessible interstitial sites of θ' give a high Cu mobility inside the phase, which we observe through two forms of structural modifications: (i) The formation of stacking faults, in particular on $\{101\}_{\theta'}$ planes. These are predominantly found regularly spaced, 828 pm apart, which forms a new superstructure θ'_{D} with space group C2/m and composition Al_5Cu_3 (on full occupation). (ii) Irradiation by the electron beam in a TEM induces vacancy–interstitial pairs which after short exposures at both 80 and 200 kV disrupt the pattern of Cu in $\theta/\theta'_{\mathrm{D}}$, presumably resulting in a non-ordered Cu distribution. With our methodology of calculating the damaging rate, based on NEB–DFT simulations and the Mott model for the knock-on damage interaction cross-section, we find a qualitative agreement with the experimental trend that θ'_{D} is more easily damaged than θ', and that electrons are more damaging at 200 kV than at 80 kV in both structures. Small structural modifications, exemplified here with $\theta' \rightarrow \theta'_{\mathrm{D}}$, can greatly increase the sensitivity to irradiation.

Funding

The authors would like to thank the Research Council of Norway (RCN) for funding of the FRINATEK project "Fundamental investigations of precipitation in the solid state with focus on Al-based alloys". The research was supported by the project NORTEM (Grant 197405) within the programme INFRASTRUCTURE of the RCN. NORTEM was co-funded by the RCN and the project partners NTNU, UiO and SINTEF.

References

[1] A. Wilm, Metallurgie 8 (1911) p. 225.
[2] P.D. Merica, R.G. Waltenberg and H. Scott, Sci. Pap. Bur. Stand. 15 (1919) p. 271.
[3] S.C. Wang and M.J. Starink, Int. Mater. Rev. 50 (2005) p. 193.
[4] V. Gerold, Scripta Metall. 22 (1988) p. 927.
[5] F. Gayle and M. Goodway, Science 266 (1994) p. 1015.
[6] T. Sato and A. Kamio, Mater. Sci. Eng. A 146 (1991) p. 161.
[7] L. Bourgeois, C. Dwyer, M. Weyland, J.F. Nie and B.C. Muddle, Acta Mater. 59 (2011) p. 7043.
[8] J.M. Silcock, T.J. Heal and H.K. Hardy, J. Inst. Met. 82 (1953) p. 239.
[9] C. Laird and H.I. Aaronson, Acta Metall. 15 (1967) p. 660.
[10] S. Wenner, C.D. Marioara, S.J. Andersen, M. Ervik and R. Holmestad, Mater. Charact. 106 (2015) p. 226.
[11] G. Kresse and J. Hafner, Phys. Rev. B 47 (1993) p. 558.
[12] G. Kresse and J. Furthmüller, Phys. Rev. B 54 (1996) p. 11169.
[13] G. Kresse and D. Joubert, Phys. Rev. B 59 (1999) p. 1758.
[14] J.P. Perdew, K. Burke and M. Ernzerhof, Phys. Rev. Lett. 77 (1996) p. 3865.
[15] M. Methfessel and A.T. Paxton, Phys. Rev. B 40 (1989) p. 3616.
[16] Henkelman and H. Jónsson, J. Chem. Phys. 113 (2000) p. 9901.

[17] Henkelman and H. Jónsson, J. Chem. Phys. 113 (2000) p. 9978.
[18] P. Ehrhart and U. Schlagheck, J. Phys. F: Met. Phys. 4 (1974) p. 1575.
[19] M.D. Rossell, R. Erni, M. Asta, V. Radmilovic and U. Dahmen, Phys. Rev. B 80 (2009) p. 024110.
[20] F. Wang, J. Graetza, S. Moreno, C. Ma, L. Wu, V. Volkov and Y. Zhu, ACS Nano 5 (2011) p. 1190, supporting information.
[21] P. Jung, Phys. Rev. B 23 (1981) p. 664.
[22] L. Kovarik, S.A. Court, H.L. Fraser and M.J. Mills, Acta Mater. 56 (2008) p. 4804.
[23] S. Kajiwara, J. Phys. Soc. Jpn 26 (1969) p. 339.
[24] G.C. Weatherly, Acta Metall. 18 (1970) p. 15.
[25] L. Bourgeois, N.V. Medhekar, A.E. Smith, M. Weyland, J.F. Nie and C. Dwyer, Phys. Rev. Lett. 111 (2013) p. 046102.
[26] M. Iyer, V. Gavini and T.M. Pollock, Phys. Rev. B 89 (2014) p. 014108.
[27] R. Sankaran and C. Laird, Mater. Sci. Eng 15 (1974) p. 159.
[28] G. Lucas and L. Pizzagalli, Nucl. Instrum. Meth. B 229 (2005) p. 359.